Applied Catalysis B: Environmental 176–177 (2015) 1–10

Contents lists available at ScienceDirect

Applied Catalysis B: Environmental

journal homepage: www.elsevier.com/locate/apcatb

Kinetics of the dehydration of glycerol over acid catalysts with an investigation of deactivation mechanism by coke

Hongseok Park, Yang Sik Yun, Tae Yong Kim, Kyung Rok Lee, Jayeon Baek, Jongheop Yi*

World Class University Program of Chemical Convergence for Energy & Environment, School of Chemical and Biological Engineering, Institute of Chemical Processes, Seoul National University, Seoul 151-742, Republic of Korea

ARTICLE INFO

Article history:
Received 8 October 2014
Received in revised form 19 March 2015
Accepted 22 March 2015
Available online 24 March 2015

Keywords:
Dehydration of glycerol
Kinetics
Deactivation
Acid catalysts

ABSTRACT

Kinetics for the dehydration of glycerol, taking deactivation into account, was investigated. HZSM-5 and ASPN-40 (aluminosilicophosphate nanosphere) catalysts were used in the studies. A kinetic model was established, based on the reaction mechanism, taking into account two parallel reactions (transformation of glycerol into acrolein or acetol) that occur over the acid sites. The results were consistent with experimental results using both catalysts. Based on the overall reaction, the apparent kinetic parameters were obtained and the results confirmed that the first dehydration step, which occurs over Brønsted acid sites, is the rate determining step. In addition, the structural features of catalysts appear to be one of the crucial factors that affect the kinetics of the reaction over acid sites. The HZSM-5 and ASPN-40 catalysts were deactivated to different degrees under same conditions. A kinetic equation for the deactivation, which is a function of product concentration, was found to be in good agreement with the experimental results. To elucidate the mechanism of catalyst deactivation, various characteristic analyses (BET, NH_3-TPD, TPO, and ^{13}C NMR) were employed. The changes in the properties of catalysts and the nature of the produced coke were analyzed. In the case of HZSM-5, the condensation of coke precursors is promoted within its narrow pore structures, which results in the rapid deactivation of the catalyst. In ASPN-40, less condensed carbonaceous compounds are observed and the deactivation is delayed due to the relatively uninterrupted diffusion of materials (reactants, products, or potential coke precursors).

1. Introduction

As concerns regarding the depletion of fossil fuels and environmental issues continue to grow, great efforts have been made to develop alternate conventional petrochemical-based processes. Glycerol, which is generated through the trans-esterification step in the production of biodiesel, represents a promising feedstock not only owing to its eco-friendly and sustainable properties, but also its multifunctional structure [1–4]. Using catalysts, glycerol can be transformed into a wide spectrum of hydrocarbons, aldehydes, and alcohols. Among them, acrolein is considered to be one of the most essential intermediates in the chemical industry for producing acrylic acid [5,6]. Acrolein is currently produced through an oxidation process from petrochemical-based propylene [7,8]. However, soaring costs of fossil fuels and demands for acrylic acid provide a strong motivation to develop alternative processes for producing acrolein via the acid-catalyzed dehydration of glycerol.

Consequently, a number of studies have focused on the design and development of effective acid catalysts for the dehydration of glycerol. Heterogeneous catalyst systems, such as solid acid catalysts, supported heteropolyacids (HPA) [9,10], zeolites [11,12], mixed metal oxides [13,14], phosphates [15], and pyrophosphates [16] have been the major object in such studies. Also, excellent catalytic performance for the reaction involving the use of HPA and zeolites, with acrolein selectivity of up to 98% and around 70%, respectively [10,12]. Through the intensive analyses, it is generally acknowledged that performance is dominantly affected by the both textural and acidic properties of the acid catalyst used [9–16]. However, a common and critical problem associated with the abovementioned catalysts is their rapid deactivation, which is the major hurdle to overcome for successful industrial application. According to previous studies, attempting to clarify the causes of deactivation, the nature of the accumulated carbonaceous compounds, which may be formed by sequential reactions from either reactant or product, are issues that need to be solved [17–21].

Since much attention has started to be paid to the dehydration of glycerol over acid catalysts, many possible mechanisms for the main reactions or deactivation have been proposed and

* Corresponding author. Tel.: +82 2 880 7438.
E-mail address: jyi@snu.ac.kr (J. Yi).

http://dx.doi.org/10.1016/j.apcatb.2015.03.046
0926-3373/

various characteristic analyses of catalysts or coke have been carried out [17,21–23]. However, to the best of our knowledge, a kinetics-based investigation of the catalytic reaction, taking deactivation into account, has been missing in most cases till date. Kinetic modeling can play an important role in unraveling a reaction mechanism, analyzing the quantitative effects of catalytic properties on reaction rates, and even developing a stable catalyst with a high activity. Especially, in the case of a reaction, such as glycerol dehydration, in which rapid catalyst deactivation by coke formation occurs, a proper kinetic model describing the deactivation behavior is even more highly required for practical or industrial purposes.

Herein, we report on a comprehensive kinetic study of the dehydration of glycerol over acid catalysts. Our objective was to examine catalytic deactivation via coke production with time on stream (TOS), not only quantitatively but also qualitatively. To accomplish this, microporous HZSM-5 [24] and hierarchically mesoporous ASPN-40 [25] were selected as model catalysts for their outstanding acid properties and distinctively different porous structures. The deactivation behavior is described by kinetic equations based on the possible pathways for coke formation and the suitability of the equations was tested. Using various characterization methods (BET, NH_3-TPD, TPO, and ^{13}C NMR), changes in the properties of the catalysts and the nature of coke deposits were examined with TOS. In addition, the influence of catalytic properties on the overall deactivation behavior as well as the mechanism responsible for coke formation is discussed. Prior to this, kinetic modeling for the main reaction was also established on the basis of the experimental results, in an attempt to confirm the proposed mechanisms and calculate the apparent rate constants. The findings would be expected to provide insights into the conditions for using the catalysts and the effects of porous structure and acid properties on the reaction kinetics.

2. Experimental

2.1. Preparation and characterization of catalysts

HZSM-5 (Si/Al ratio = 40) was prepared through the calcination of commercial zeolite NH_4ZSM-5(Zeolyst, product no. = CBV 8014) at 550 °C for 6 h. ASPN-40 (Si/Al ratio = 40) was prepared by the method reported in our previous work [25].

The N_2 adsorption–desorption isotherms were measured at −196 °C using a Micrometrics ASAP-2010 apparatus. The pore size distribution curves were calculated by the Barrett–Joyner–Halenda (BJH) method using the adsorption branches of the isotherms. The carbon content of the used samples was determined by CHNS elemental analysis using a CHNS-932 analyzer. NH_3-TPD was performed on a conventional apparatus. A 0.1 g sample was pretreated with 10.2% NH_3/He gas at 50 °C. The temperature was increased to 100 °C and maintained for 1 h under He in order to eliminate physically adsorbed NH_3. The temperature was cooled to 50 °C and increased again to 800 °C (10 °C min^{-1}) under He. Simultaneously, the desorbed NH_3 (m/z = 16) was quantitatively detected. For the TPO analysis of used catalysts, the sample was treated at 100 °C for 1 h. Under He atmosphere, physically adsorbed molecules on the used catalysts were expected to be desorbed or volatilized. After the pretreatment, the temperature was decreased to 50 °C. The signal of CO_2 and CO (m/z = 44 and 28) was monitored by a mass spectrometer while temperatures increased up to 800 °C at a rate of 10 °C min^{-1} under a flow of 10% O_2/He. Solid state ^{13}C CP-MAS NMR data were collected on a AVANCE 400 WB spectrometer. The samples were rotated at 7 kHz. The pulse sequence was a frequency of 100.7 MHz and a spectral width of 31 kHz.

2.2. Catalytic reaction

The dehydration of glycerol was carried out under atmospheric pressure at 250–300 °C. The catalyst was placed in a vertical quartz reactor with an inner diameter of 8 mm. Before the reaction, the catalyst was pretreated at 250 °C under a mixed flow of He (25 mL min^{-1}) and N_2 (2.93 mL min^{-1}) for 1 h. He was used as a carrier gas and N_2 was used as an internal standard in the analysis of the gas-phase products using a TCD detector. A 1.2 M (ca. 10.8 wt%) aqueous solution of glycerol was fed at a rate of 2 mL h^{-1} and vaporized. The resulting vapor was mixed with the flow of He and N_2 and then passed through the catalyst bed. The molar ratio of glycerol:H_2O:N_2:He was 1:42.3:3:25.5. The contact time τ (W/F), where W is weight of catalyst (g) and F is molar flow rate of reactant (mol h^{-1}), is controlled by the amount of catalysts from 2.08 $g_{catalyst}$ h mol^{-1} to 104.17 $g_{catalyst}$ h mol^{-1}. To reduce the temperature gradient caused by heat transfer during the reaction tests even at high contact time and conversion, both of reactant and catalysts were diluted. The molar ratio of glycerol was kept at low level and silicon carbide (SiC); an inert material with high heat conductivity, was loaded on the reactor with the catalysts. The reaction products were collected by a cold trap after passing through a con-

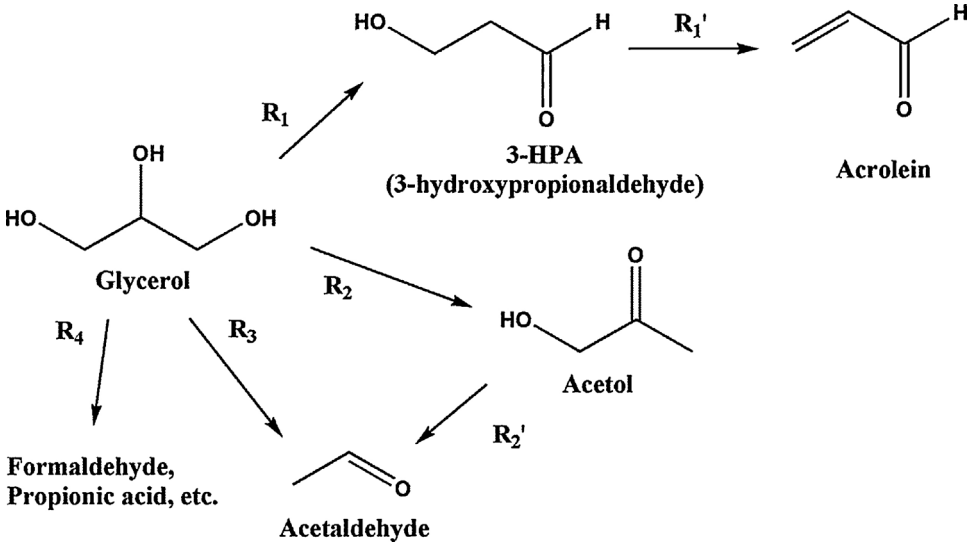

Scheme 1. The reaction pathway of the dehydration of glycerol over solid acid catalysts.

denser. 1-Propanol was the internal standard in the analysis of the collected products by a gas chromatograph (Younglin ACME 6500 model) equipped with a FID detector. The liquid product sample was collected for 30 min after the reaction and then analyzed.

3. Results and discussion

3.1. Kinetic modeling of the dehydration of glycerol

Plausible reaction routes for glycerol dehydration in the gas phase over solid acid catalysts have been reported in many studies [10,17,26–29]. Based on the obtained product distribution, a possible reaction pathway over the catalysts used in this study is illustrated in Scheme 1. In this proposed pathway, glycerol is mainly dehydrated to 3-hydroxypropionaldehyde (3-HPA, R_1) and acetol (hydroxyacetone, R_2). It has been reasonably proposed that the central hydroxyl group of glycerol is protonated on a Brønsted acid site and the former reaction begins. The protonated intermediate is converted through the liberation of a hydronium ion (H_3O^+) and undergoes rearrangement to 3-HPA [27,28]. On the other hand, the latter reaction (R_2) is initiated via a different mechanism. As a glycerol molecule approaches a Lewis acid site, the terminal hydroxyl group of glycerol interacts with the Lewis acid site. This consequently leads to the formation of an enol intermediate that rapidly rearranges to give acetol [10].

3-HPA is sufficiently reactive and readily converted into acrolein through a second dehydration step (R_1') with high selectivity. On the other hand, acetol can be transformed into acetaldehyde (R_2') through C—C cleavage. Acetaldehyde can be also derived from glycerol through consecutive dehydrogenation and dehydration (R_3) reactions [17,30]. In actual experiments, a wide range of products, including formaldehyde, 1,3-dioxan-5-ol, 1,3-dioxolan-4-yl-methanol, and allyl alcohol were detected by GC–MS but the concentration of each compound was negligible. Due to the variety of products, the minor byproducts were grouped into a lump and the route involved in the conversion of glycerol to minor byproducts are denoted as R_4 in Scheme 1.

As shown in Fig. 1, glycerol is dominantly converted into acrolein, acetol, and acetaldehyde over HZSM-5 and ASPN-40. Therefore, the reaction steps (R_1–R_4 and R_1'–R_2') were principally taken into account to describe the catalytic reaction on the basis of the scheme represented above.

For a comparative study between HZSM-5 and ASPN-40 in terms of apparent kinetics, the external mass transfer effect on both catalysts was tested at 250 °C. It was found that there was practically no change in the glycerol conversion (48–49%), while varying He flow rate from 25 mL min^{-1} to 50 mL min^{-1}, the total flow rate from 69.9 to 94.9 mL min^{-1} at W/F ratio equal to 4.17 and 8.33 $g_{catalyst}$ h mol^{-1} for HZSM-5 and ASPN-40, respectively. Thus, it was found that the external mass transfer resistance was negligible.

On the basis of heterogeneous kinetic modeling in the supplementary material, simplified kinetic model for the dehydration of glycerol was developed assuming to be first order to the reactant. Among the reaction routes, water molecules are released during the dehydration steps. However, the total amount of water can be assumed to be constant due to excessively large proportion of water and the low concentration of glycerol in the feeding solution. Thus, the dehydration steps are assumed to be pseudo-first-order reactions.

The reaction rate of each step is described as following equations,

$$\frac{dC_{glycerol}}{d\tau} = -(k_1 + k_2 + k_3 + k_4)\, C_{glycerol} \quad (1)$$

$$\frac{dC_{3-HPA}}{d\tau} = k_1 C_{glycerol} - k_1' C_{3-HPA} \quad (2)$$

$$\frac{dC_{acrolein}}{d\tau} = k_1' C_{3-HPA} \quad (3)$$

$$\frac{dC_{acetol}}{d\tau} = k_2 C_{glycerol} - k_2' C_{acetol} \quad (4)$$

$$\frac{dC_{acetaldehyde}}{d\tau} = k_3 C_{glycerol} + k_2' C_{acetol} \quad (5)$$

$$\frac{dC_{lump}}{d\tau} = k_4 C_{glycerol} \quad (6)$$

where k_i represents pseudo first order kinetic rate constant of R_i and C_j is mole fraction of j component. The above ordinary differential equations (ODEs) are functions of the contact time τ and calculated using Matlab function ODE45 based on Runge–Kutta method. The optimization function "fminsearch" was employed to minimize the objective function, sum of the square of errors, $\Phi = \Sigma(X_{i,cal} - X_{i,exp})^2$, for the estimation of parameters related to reaction rate and activation energy. $X_{i,exp}$ is the experimental values for the component or the lump and $X_{i,cal}$ is the calculated values.

Fig. 1 shows the calculated curves and experimental data obtained at different reaction temperatures (250, 275, and 300 °C). In the given range of reaction temperatures, the distribution of products is barely affected once the contact time is sufficiently high for the complete conversion of glycerol. Overall, the yield of acrolein shows trend of reaching maximum at some point with the yield being maintained. This trend is more remarkable as the contact time increases, however, the amount of acetol produced decreases after reaching its maximum and the yield of acetaldehyde is subsequently increased. This implies that the further degradation of acrolein is minimal through the catalyst bed whereas acetol tends to be transformed into small compounds, such as acetaldehyde as represented in Scheme 1.

As shown in Fig. 1, the kinetic model describing the reaction over the catalysts fits well to the experimental data and the kinetic parameters were determined from the calculated curves. The R^2 values for each curves in Fig. 1 was within range of 0.84–0.98. The apparent rate constants are interpreted as lumped parameters involving internal diffusion, adsorption, desorption, and intrinsic reaction rate constants. The apparent activation energies were calculated through Arrhenius plots (Fig. S1) on the basis of the reaction rates within the range of temperatures (250–300 °C). These estimated values for the apparent rate constant and the corresponding apparent activation energy are summarized in Table 1. Because of the high reactivity of 3-HPA, it was barely detected in experiments, and its mole fraction at the exit of the reactor would be expected to be negligible under the conditions used in this study. This indicates that the second dehydration step (3-HPA to acrolein, R_1') in the reaction sequence to produce acrolein from glycerol (Scheme 1) proceeds much faster than the primary dehydration step (glycerol to 3-HPA, R_1). Therefore, it can be concluded that the rate of acrolein production is strongly dependent on the rate constant of the first dehydration step (k_1).

As listed in Table 1, when the reaction temperature is increased from 250 °C to 300 °C, the rate constant for each reaction correspondingly increases. Over the HZSM-5 and ASPN-40 catalysts, the rate constant k_1 (glycerol to acrolein via 3-HPA) is higher than the rate constant k_3 (glycerol to acetol) at the any of the investigated temperatures. On the basis of the mechanism shown in Scheme 1, the reaction rate for the dehydration step on Brønsted acid sites (R_1) is significantly faster than that on Lewis acid sites (R_2). Considering the amount of Brønsted and Lewis acid sites on HZSM-5 (0.376 and 0.099 mmol g^{-1}) and ASPN-40 (0.308 and 0.106 mmol g^{-1}) calculated from data reported in a previous study [25], the reaction rate on a single Brønsted acid site (R_1) is 20 and 5 times faster than that on a single Lewis acid site (R_2) of HZSM-5 and ASPN-40, respectively. This can be also related with the differences between

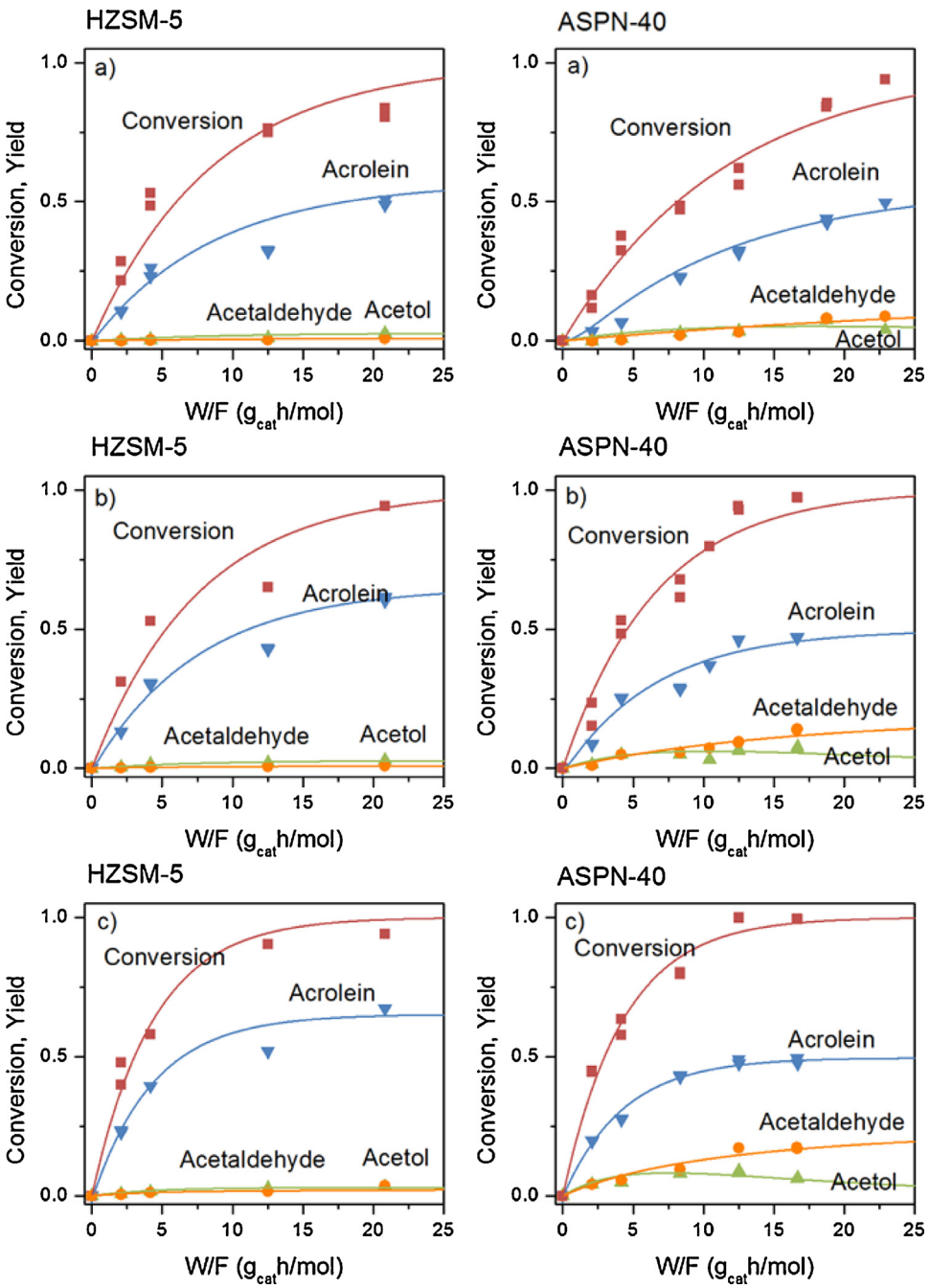

Fig. 1. Comparison of experimental results (points) and data fitted for the model (lines) above for the dehydration of glycerol over HZSM-5 and ASPN-40 at (a) 250, (b) 275, and (c) 300 °C.

reaction mechanisms over Brønsted and Lewis acid site. Unlike the protonation step on a Brønsted acid site, the interaction of a glycerol molecule with a Lewis acid site is affected by steric hindrance [10]. Additionally, the reaction rates for the primary dehydration steps (R_1 and R_2) over ASPN-40 are more sensitive to the reaction temperature compared to that for HZSM-5. It would be expected that the pore structure of the catalyst is a potential factor affecting the reaction rates. The hierarchically mesoporous structure of ASPN-40 [25] has an advantage in terms of mass transfer. With an elevated reaction temperature, the active sites of ASPN-40 are more readily accessible to reactant molecules while, in the case of HZSM-5, the effect of temperature on the mobility of reactant molecules is limited by the narrow pore structure and may lead to undesired reactions. The rate of acetaldehyde production is mainly determined by k_4 and k_5. As reaction temperature increases, the effect of the degradation of glycerol (R_3) [30] gradually become dominant to produce acetaldehyde over both the HZSM-5 and ASPN-40 catalysts.

3.2. Deactivation behavior

In spite of the high initial activity of HZSM-5 and ASPN-40, it is well known that unavoidable deactivation is mainly due to coke formation from sequential reactions of the reactants or products on the surface active sites [17–21,31]. As shown in Fig. 2, catalytic activity decreases with TOS, depending on the catalysts. Due to the

Table 1
Apparent kinetic parameters for the dehydration of glycerol over HZSM-5 and ASPN-40 catalysts calculated by the best fitted curve.

Reaction rate constant (mol/$g_{catalyst}$ h)	Reaction temperature (°C)			Activation energy (kJ/mol)
	250	275	300	
HZSM-5				
k_1	6.618×10^{-2}	8.575×10^{-2}	1.497×10^{-1}	40.4
k_2	3.109×10^{-3}	3.916×10^{-3}	7.690×10^{-3}	44.8
k_2'	1.370×10^{-2}	1.843×10^{-2}	5.715×10^{-2}	70.5
k_3	9.830×10^{-3}	$1.028\times^{-2}$	4.013×10^{-2}	69.1
k_4	4.538×10^{-2}	4.747×10^{-2}	6.818×10^{-2}	33.9
ASPN-40				
k_1	4.741×10^{-2}	7.539×10^{-2}	1.161×10^{-1}	44.6
k_2	8.301×10^{-3}	1.674×10^{-2}	3.139×10^{-2}	66.6
k_2'	5.062×10^{-3}	1.159×10^{-2}	2.265×10^{-2}	74.7
k_3	3.164×10^{-2}	5.552×10^{-2}	6.510×10^{-2}	36.2
k_4	2.450×10^{-2}	4.797×10^{-2}	6.328×10^{-2}	48.0

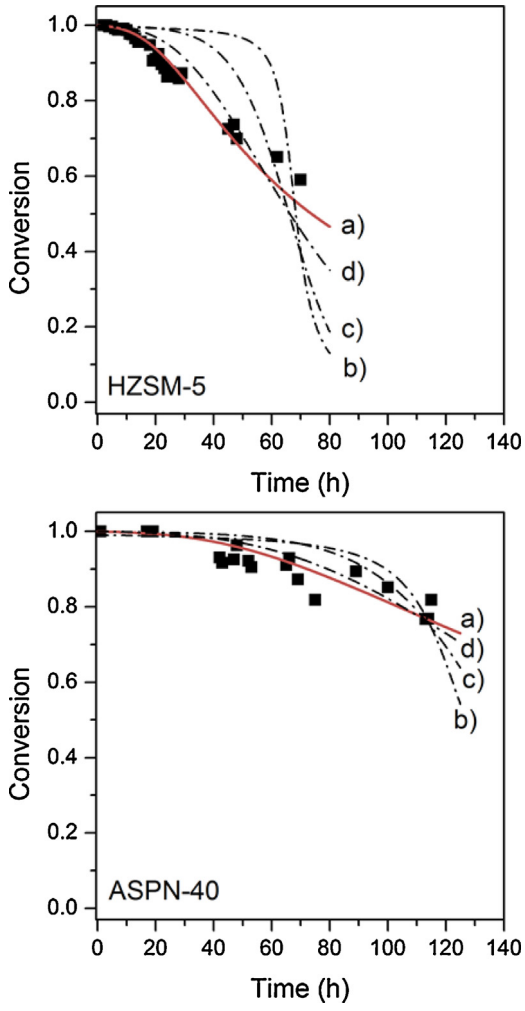

Fig. 2. Identification of kinetic models describing the deactivation of HZSM-5 and ASPN-40: experimental results (points) and curves fitted for the models depending on the concentration of (a) products (solid line, red), (b) the reactant, (c) both, and (d) regardless of the fraction of the stream. The reaction data were obtained with time on stream under the following conditions: temperature, 250 °C; contact time (W/F), 83.33 $g_{catalyst}$ h mol^{-1}; feed flow rate, 2 mL h^{-1} of aqueous solution of glycerol (1.2 M); inert gas flow rate, 25 mL min^{-1} of He and 2.93 mL min^{-1} of N_2. (For interpretation of the references to color in this figure legend, the reader is referred to the web version of this article.)

diversity of the number of potential coke precursors a quantitative analysis of deactivation behavior becomes difficult, which leads simple kinetic models being proposed based on possible causes of coke formation.

3.2.1. Kinetic study of deactivation

A kinetic model for the deactivation behavior of the acid catalysts is based on the observed decrease in glycerol conversion with TOS. A general description of catalyst deactivation, which is represented by the mean integral activity, was proposed in a previous study [32]. In a fixed bed catalytic system, due to the difficulties in analyzing the activity of individual acid sites, it is rational to describe the catalytic deactivation as a decrease in the mean integral activity ($\langle a\rangle$). It is defined as the integration of the activity, a, with respect to the dimensionless height (h) (Eq. (7)).

$$\langle a\rangle = \int_0^1 a(h)\mathrm{d}h \tag{7}$$

To modify the general expression for catalytic deactivation, the conversion rate of glycerol into primary products (Eq. (1)) over the acid catalysts was assumed to be a first order reaction like Eqs. (8) and (9) where k is glycerol consumption rate constant and $X_{glycerol}$ is glycerol conversion.

$$r_{glycerol} = \frac{\mathrm{d}C_{glycerol}}{\mathrm{d}\tau} = -kC_{glycerol}\langle a\rangle \tag{8}$$

$$\frac{\mathrm{d}X_{glycerol}}{\mathrm{d}\tau} = k(1-X_{glycerol})\langle a\rangle \tag{9}$$

The above proposed deactivation model equations were derived for the following possible cases where $C_{0,glycerol}$ represents the initial mole fraction of glycerol; the rate of deactivation is dominantly dependent on the concentration of the reactant (model 1), products (model 2), or both (model 3). Also, for the case in which the catalytic deactivation proceeds regardless of composition of the flow, model 4 was considered.

Model 1

$$\frac{\mathrm{d}\langle a\rangle}{\mathrm{d}t} = -k_{d,app}C_{glycerol}\times\langle a\rangle = -k_{d,app}C_{0,glycerol}(1-X_{glycerol})\langle a\rangle \tag{10}$$

$$\frac{\mathrm{d}X_{glycerol}}{\mathrm{d}t} = k_{d,app}C_{0,glycerol}(1-X_{glycerol})^2\ln(1-X_{glycerol}) \tag{11}$$

Model 2

$$\frac{\mathrm{d}\langle a\rangle}{\mathrm{d}t} = -k_{d,app}C_{0,glycerol}X_{glycerol}\langle a\rangle \tag{12}$$

$$\frac{\mathrm{d}X_{glycerol}}{\mathrm{d}t} = k_{d,app}C_{0,glycerol}X_{glycerol}(1-X_{glycerol})\ln(1-X_{glycerol}) \tag{13}$$

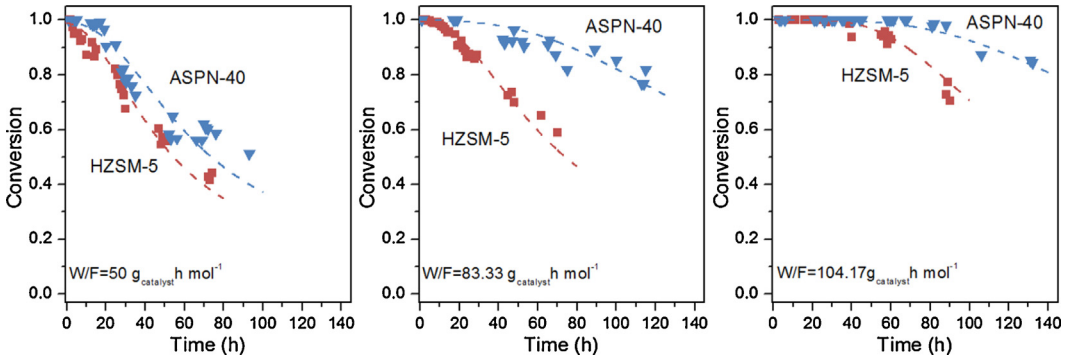

Fig. 3. Comparison of experimental results (points) and those fitted for the deactivation kinetic model (dashed lines) for the dehydration of glycerol over HZSM-5 and ASPN-40 with time on stream.

Model 3

$$\frac{d\langle a\rangle}{dt} = -k_{d,app}C_{glycerol}C_{products}\langle a\rangle = -k_{d,app}C_{0,glycerol}{}^{2}X_{glycerol}(1-X_{glycerol})\langle a\rangle \quad (14)$$

$$\frac{dX_{glycerol}}{dt} = k_{d,app}C_{0,glycerol}{}^{2}X_{glycerol}(1-X_{glycerol})^{2}\ln(1-X_{glycerol}) \quad (15)$$

Model 4

$$\frac{d\langle a\rangle}{dt} = -k_{d,app}C_{0,glycerol}\langle a\rangle \quad (16)$$

$$\frac{dX_{glycerol}}{dt} = k_{d,app}C_{0,glycerol}(1-X_{glycerol})\ln(1-X_{glycerol}) \quad (17)$$

Fig. 2 shows the conversion of glycerol over HZSM-5 and ASPN-40 with TOS under the same conditions. The experimental results (points) are compared with the calculated values (dashed lines), obtained using the deactivation models. As observed in Fig. 2, the best fit for the conversion of glycerol was obtained for a model which is dependent on the concentration of products and R^2 values are listed in Table S1 for a clear discrimination of each model. At various contact times controlled by the amount of catalyst (0.12–0.25 g), the calculated curves were found to fit well with the experimental results (Fig. 3) and the suitability of a model equation for the deactivation behavior was confirmed. The apparent deactivation rate constants ($k_{d,app}$) calculated from the best fit are listed in Table 2.

Table 2
Deactivation rate constant for the dehydration of glycerol over HZSM-5 and ASPN-40 catalysts.

HZSM-5		ASPN-40	
W/F ($g_{catalyst}$ h mol^{-1})	$k_{d,app}$ (h^{-1})	W/F ($g_{catalyst}$ h mol^{-1})	$k_{d,app}$ (h^{-1})
50	2.98	50	2.56
83.33	2.55	83.33	0.88
104.17	1.35	104.17	0.71

On the basis of the kinetic model for the catalyst deactivation, it appears that this is due to the formation of carbonaceous compounds, which are generated through consecutive reactions from

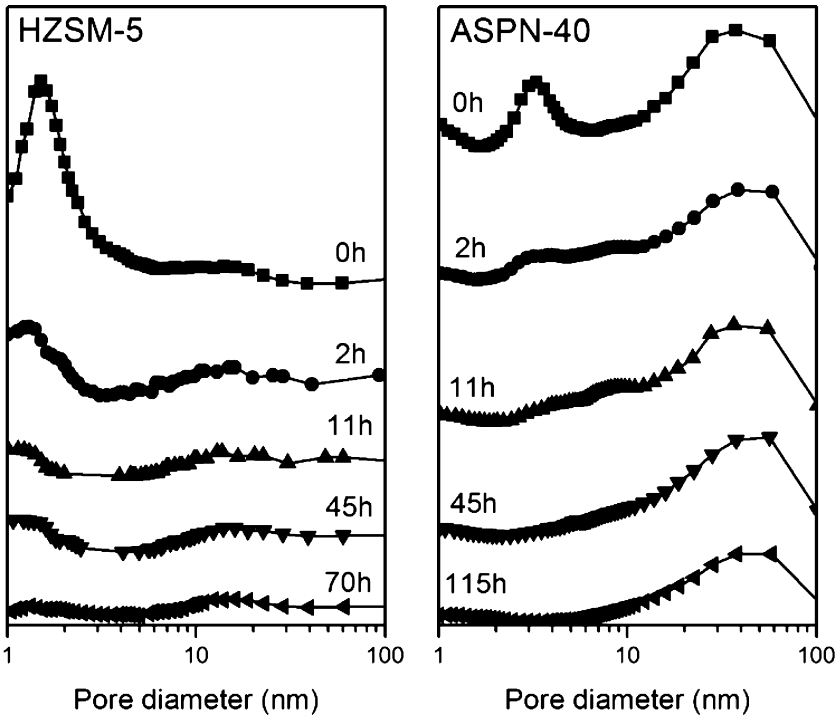

Fig. 4. Comparison of BJH pore size distribution of the used HZSM-5 and ASPN-40 catalysts with the course of time.

primary products. As previously reported, a considerable amount of coke is formed on the acid catalysts when the initial dehydration products (3-HPA and acetol) are converted, whereas less coke deposits are observed when glycerol is dehydrated over the same acid catalysts [17].

From Fig. S2, the yield of acrolein is largely affected by the decrease of catalytic activity, whereas the yield of other byproducts remains at a relatively low level with TOS. This suggests that Brønsted acid sites are mainly deactivated as the catalytic reaction proceeds. Owing to the high proportion of Brønsted acid sites on HZSM-5, the potential coke precursors are likely to be derived from 3-HPA and/or acrolein. Within its narrow pores, the limited diffusion of products would eventually be responsible for the consecutive reactions resulting in the formation of heavy compounds [17,33]. In the case of ASPN-40, apart from the high yield for acrolein, a considerable amount of glycerol is transformed into acetol and acetaldehyde as seen above (Figs. 1 and S2). Therefore, it would be expected that the formation of coke on ASPN-40 can be partially attributed to the oligomerization and condensation of the rather small compounds as well.

3.2.2. Changes in the nature of the used catalysts

The chemical and structural properties of catalysts have a substantial impact on the nature of coke formed in the different mechanistic pathways, and vice versa [34,35]. Based on the proposed reaction pathway and the above kinetic model for the deactivation of the catalysts, comprehensive observations of the changes in catalytic properties and the characteristics of the deposited coke are indispensable for understanding the details of the deactivation behavior of the acid catalysts.

Catalytic tests were conducted under same conditions ($W/F = 83.33\ g_{catalyst}\ h\ mol^{-1}$, $T = 250\ ^{\circ}C$) over HZSM-5 and ASPN-40. The tests were stopped after 2, 11, 45, and 70 h (115 h for ASPN-40) on stream and the used catalyst samples were collected for further investigations. Carbon content deposited on the used catalysts during the reaction time is shown in Table 3. In the case of HZSM-5, carbon content increased abruptly at the initial stage but the rate of formation of carbon species on the catalysts became significantly slow with reaction time. On the contrary, the proportion of carbon compounds on the ASPN-40 catalyst progressively increased. The trend for the increase in carbonaceous compounds on the catalysts is consistent with the changes in the textural properties. For HZSM-5, the BET surface area and micropore volume (Table 3) were decreased by more than 90% of the initial value (from 467 to 35 $m^2\ g^{-1}$ and 0.177 to 0.012 $cm^3\ g^{-1}$, respectively) within 11 h in parallel with the increase in carbon content.

According to the changes in the pore size distribution with the time (Fig. 4, left), pores with size in the range of 1–3 nm disappeared completely soon after the commencement of the catalytic reaction. This indicates that the coke deposits have a substantial effect on the textural properties of HZSM-5 by blocking the micropores of the catalyst. In contrast, ASPN-40 showed a relatively high surface area and pore volume (123 $m^2\ g^{-1}$ and 0.426 $cm^3\ g^{-1}$, respectively) even after a 115 h run. The multimodal pore distribution of ASPN-40 is initially observed in Fig. 4 (right). With the increasing TOS, its large mesopores (10–50 nm) were maintained and were essentially not affected by coke formation while relatively small pores (2–10 nm) disappeared significantly within 11 h. From the experimental results, it can be concluded that small-sized pores that are present on HZSM-5 and ASPN-40 are blocked first. The loss of porosity leads to a decrease in surface area as well a decrease in the number of active sites. Thanks to the hierarchical pore structure [25], ASPN-40 suffered less than HZSM-5 from the severe pore blockage by coke even after the large amounts of carbon species had been generated. The average pore diameter of the catalysts (Table 3) increased steadily with TOS since the blockage of micropores leads to a comparatively high contribution of the remaining mesopores and even macropores within the particles of the used catalysts.

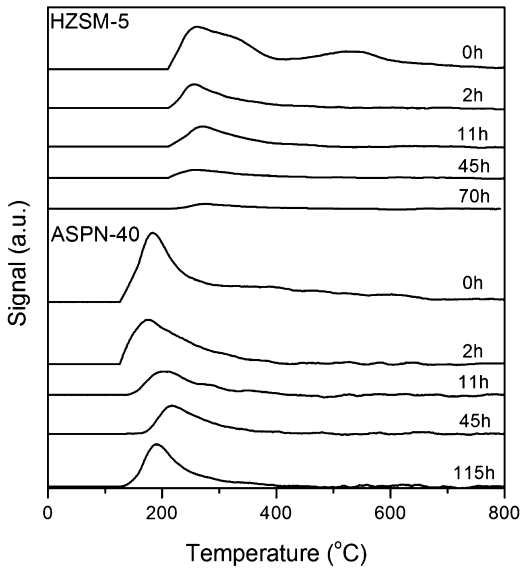

Fig. 5. NH_3-TPD profiles of the used HZSM-5 and ASPN-40 at different TOS.

To investigate the amounts and strength of the acid sites of the catalysts, temperature-programed desorption (TPD) of NH_3 experiments were carried out. As shown in the NH_3-TPD profiles of Fig. 5, the number of acid sites over HZSM-5 and ASPN-40 decreased with increasing TOS. In particular, the strong acid sites of HZSM-5, which are found in the range between 500 and 600 °C, had essentially disappeared, after a 2 h-run. This observation is in good agreement with the rapid increase of carbonaceous compounds (Table 3) that was found during the early hours of the run, since coke formation on surface of the catalysts is largely contributed by strong acid sites [27]. After 70 h of TOS, the loss of acidity in HZSM-5 reached almost 95% whereas approximately 50% of the initial acid sites in ASPN-40 remained, even after 115 h.

In addition to the aforementioned deterioration of the textural and acidic properties of the catalysts, carbonaceous deposits on the catalysts were characterized by temperature-programmed oxidation (TPO). In order to avoid any misinterpretation of the above results caused by the possible modification of coke, the reaction temperature during TPO analysis and the characteristics of carbon deposits on the used catalysts were analyzed by ^{13}C NMR after TPO at temperatures up to 500 °C. In Fig. S3, the observed changes are attributed to the oxidation of carbon compounds. In fact, most of the carbon species, such as aliphatic compounds formed during reaction were likely to be oxidized while the aromatized compounds of the used samples partly remained. It can be inferred that the carbonaceous compounds gasified to CO_2 or CO via oxidation process under 500 °C are mostly likely aliphatic species rather than aromatics.

The CO_2 and CO evolution profiles for the used HZSM-5 and ASPN-40 for various TOS are presented in Fig. 6(a) and (b), respectively. Both of the CO_2 and CO evolution curves for the used HZSM-5 samples appear to contain two peaks, and thus, deconvolution into Gaussian peaks was carried out in order to differentiate the two peaks for the oxidized carbon compounds. Based on the results shown in Fig. S3, further aromatization and polymerization of carbon deposits during TPO analysis were not detected. Therefore, the different trend of TPO curves can be interpreted as the characteristic nature of carbon deposits within each catalyst.

In Fig. 6(a), during the initial period, one is found in the lower temperature range (360–450 °C) and the other is in the higher

Table 3
Textural properties and total carbon contents of the used HZSM-5 and ASPN-40 at different TOS.

Time [h]	S_{BET} [$m^2\ g^{-1}$]	D_{ave} [nm]	S_{micro} [$m^2\ g^{-1}$]	V_{micro} [$cm^3\ g^{-1}$]	V_{total} [$cm^3\ g^{-1}$]	Carbon contents [%]
HZSM-5						
0	467	1.5	377	0.177	0.29	0
2	162	3.2	129	0.061	0.128	8.9
11	35	5.3	25.6	0.012	0.047	10.18
45	26	6.2	16.3	0.007	0.040	10.68
70	30	6.4	9.39	0.003	0.049	11.82
ASPN-40						
0	503	6.7	58	0.025	1.05	0
2	327	9.8	–	–	0.803	5.37
11	256	11.3	–	–	0.729	7.14
45	193	13.7	–	–	0.661	9.18
115	123	13.9	–	–	0.426	16.19

temperature range (490–570 °C). It should be noted that peaks for the carbon species are slightly shifted to the higher temperature region with increasing reaction time. The peak appeared initially in the range between 360 and 450 °C disappears and a new, relatively intense peak appears at an even higher temperature region over 600 °C after 70 h of TOS. The CO evolution profiles show the similar tendency with that of CO_2 but a peak with high intensity was observed at high temperature range (550–600 °C).

These experimental results are closely related to the location of coke formation and catalytic properties [36,37]. Due to the microporous structure of HZSM-5, carbonaceous compounds formed inside the pores are limited to migrating to the external surface. Consequently, the stagnant diffusion of the carbon species within the micropores leads to the formation of highly condensed and bulky hydrocarbons [38]. Additionally, the potential coke precursors (aromatics and olefins) further react with either internal or external coke and evolve to produce the heavier carbon species such as polyaromatics. These coke materials can easily block the pores and the rate of coke formation becomes slower compared with the initial period. This is in good agreement with changes in textural properties (Table 3 and Fig. 4) representing a rapid decrease in microporosity.

Importantly, TPO curves of CO_2 and CO for the ASPN-40 catalyst displayed in Fig. 6 are more distinctively deconvoluted as two peaks. A significant increment in intensity, especially for the higher temperature range (450–550 °C), can be seen after 115 h without a significant peak shift. This suggests that the amount of the carbonaceous deposits increase on the ASPN-40 catalyst without severe coke development caused by polymerization and/or oligomerization as the catalytic reaction proceeds longer. In the presence of dominant mesopores of ASPN-40, most carbon species would be expected to be deposited preferentially on the mesopores and have higher H/C ratio (less developed) due to relatively uninterrupted mass transfer [39].

The changes in the nature of carbon deposits on the surface of the HZSM-5 and ASPN-40 catalysts were also analyzed by ^{13}C NMR, as shown in Fig. 7. It has been reported that the two broad bands at 129 ppm and 35 ppm can be assigned to aromatic and aliphatic carbon species, respectively [22,40–42]. Hence the carbon species that is formed on HZSM-5 during the initial period (within 2 h) can be primarily classified as aromatic compounds. It is likely that the

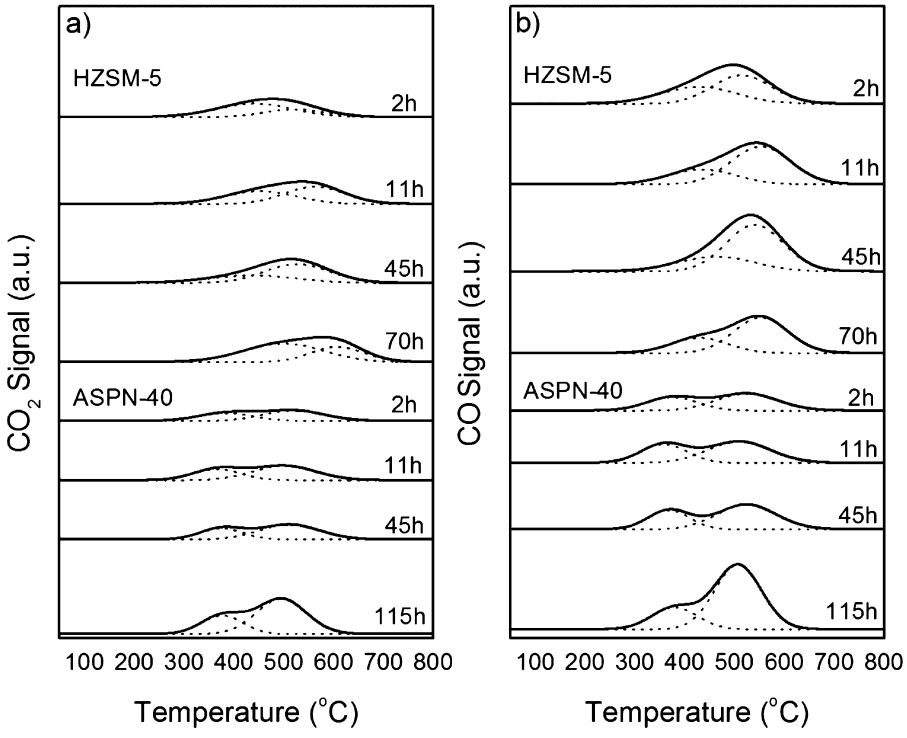

Fig. 6. TPO curves of the used HZSM-5 and ASPN-40 with the course of time.

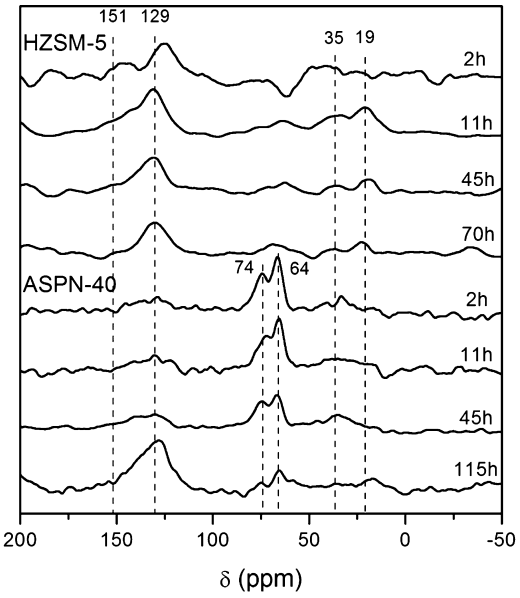

Fig. 7. ^{13}C CPMAS NMR spectra obtained for the used HZSM-5 and ASPN-40 at different TOS.

presence of strong acid sites on the fresh HZSM-5 sample promotes the aromatization of carbon species [38]. During the reaction time, a signal for aromatic carbon compounds at 125 ppm was slightly shifted to 129 ppm and a shoulder appeared at 151 ppm (after 11 h), which is assigned to substituted aromatic carbons indicating more condensation reactions [43]. A band at 19 ppm, which represents the presence of alkyl carbon compounds bound to polyaromatics [44], appeared after 11 h on steam and the intensity of the peak was maintained with increasing TOS.

On the other hand, aromatic and aliphatic compounds were hardly detected on the ASPN-40 for a short time run. However, the two peaks at 64 and 74 ppm are assigned to adsorbed glycerol or polymeric forms derived from it on the surface of the catalysts [22,45]. As the reaction time increases, the band at 129 ppm corresponding to aromatic compounds increased slightly and became remarkable after 115 h on stream, whereas the peaks at 64 and 74 ppm were decreased. This suggests that parts of the initial carbonaceous compounds, mostly adsorbed glycerol, on surface of the catalysts, are progressively transformed into various compounds including aromatics, which then accumulate on the catalyst with increasing TOS. Taking into account the results of reaction tests (Fig. 3), it can be concluded that these aromatic compounds are largely responsible for the catalytic deactivation of ASPN-40.

Through establishing kinetic equation for deactivation, we found that the deactivation of the tested catalysts can be attributed to the concentration of certain types of products and that quantitative predictions are possible. However, as the results of overall analyses of the used samples, it is consequently expected that coking proceeds via different mechanisms according to catalytic properties. The relatively more condensed and heavier carbon species within micropores of HZSM-5 are highly responsible for the rather drastic deactivation of HZSM-5. In contrast, the somewhat delayed formation of aromatic compounds within ASPN-40, which directly affects catalytic activity, appears to contribute to the long-term stability of a catalyst.

4. Conclusions

A kinetic study of the dehydration of glycerol over acid catalysts, including their deactivation by coke with TOS, was conducted. Based on the experimental results and the reaction mechanism, a kinetic model for the catalytic reaction over a commercial catalyst (HZSM-5) and a newly developed catalyst (ASPN-40) was established as the result of quantitative analyses for the product distribution. Based on the well-fitted curve to the experimental results, it is confirmed that the first dehydration step occurring over Brønsted acid site is the rate determining step for the production of acrolein. From the calculated kinetic parameters for each reaction in a range of experimental conditions (temperature, contact time), the findings show that the kinetics of the overall reaction are affected by both the structural and acidic properties of catalysts.

In addition, the kinetic description of the catalytic reaction resulted in the prediction of the mechanistic routes for the deactivation by coke. The catalytic deactivation is expressed by a comprehensive kinetic model, which is mainly dependent on the concentration of products. In spite of the dissimilar properties of the tested catalysts, the kinetic equation for deactivation permits the decrease in catalytic activity with time to be predicted. By means of characteristic analyses (BET, NH_3-TPD, TPO, and ^{13}C NMR), a further understanding of deactivation behavior and coke formation associated with catalytic properties was developed. Findings of this investigation indicate that the mechanism of coke formation and the degree of its influence on the activity is strongly dependent on catalytic properties. The kinetic description of the reaction over acid catalysts provides quantitative and qualitative analyses of the effects of the reaction conditions, catalytic properties, and even deactivation behavior with the course of time for such reactions. In addition, the critical role of catalyst design based on kinetic studies in biomass-related processes can be used for establishing a chemical process, determining of operating conditions, and improve productivity in such processes.

Acknowledgement

This work was supported by the National Research Foundation of Korea (NRF) grant funded by the Korea Government (MEST) (no. 2013R1A2A2A01067164).

Appendix A. Supplementary data

Supplementary data associated with this article can be found, in the online version, at http://dx.doi.org/10.1016/j.apcatb.2015.03.046.

References

[1] F. Ma, M.A. Hanna, Bioresour. Technol. 70 (1999) 1–15.
[2] M. Stöcker, Angew. Chem. Int. Ed. 47 (2008) 9200–9211.
[3] Z.Y. Zakaria, N.A.S. Amin, J. Linnekoski, Biomass Bioenergy 55 (2013) 370–385.
[4] R.A. Sheldon, Green Chem. 16 (2014) 950–963.
[5] J. Tichy, Appl. Catal. A 157 (1997) 363–385.
[6] J. Kunert, A. Drochner, J. Ott, H. Vogel, H. Fueß, Appl. Catal. A 269 (2004) 53–61.
[7] P. Kampe, L. Giebeler, D. Samuelis, J. Kunert, A. Drochner, F. Haaß, A.H. Adams, J. Ott, S. Endres, G. Schimanke, T. Buhrmester, M. Martin, H. Fuess, H. Vogel, Phys. Chem. Chem. Phys. 9 (2007) 3577–3589.
[8] K. Schuh, W. Kleist, M. Høj, V. Trouillet, P. Beato, A.D. Jensen, G.R. Patzke, J.D. Grunwaldt, Appl. Catal. A 482 (2014) 145–156.
[9] S.-H. Chai, H.-P. Wang, Y. Liang, B.-Q. Xu, Appl. Catal. A 353 (2009) 213–222.
[10] A. Alhanash, E.F. Kozhevnikova, I.V. Kozhevnikov, Appl. Catal. A 378 (2010) 11–18.
[11] Y.T. Kim, K.D. Jung, E.D. Park, Micropor. Mesopor. Mater. 131 (2010) 28–36.
[12] C.J. Jia, Y. Liu, W. Schmidt, A.-H. Lu, F. Schüth, J. Catal. 269 (2010) 71–79.
[13] L.-Z. Tao, S.H. Choi, Y. Zuo, W.-T. Zheng, Y. Liang, B.-Q. Xu, Catal. Today 158 (2010) 310–316.
[14] J. Deleplanque, J.L. Dubois, J.F. Devaux, W. Ueda, Catal. Today 157 (2010) 351–358.
[15] F. Wang, J.-L. Dubois, W. Ueda, J. Catal. 268 (2009) 260–267.
[16] F. Wang, J.-L. Dubois, W. Ueda, Appl. Catal. A 376 (2010) 25–32.
[17] W. Suprun, M. Lutecki, T. Haber, H. Papp, J. Mol. Catal. A: Chem. 309 (2009) 71–78.
[18] B. Katryniok, S. Paul, M. Capron, F. Dumeignil, ChemSusChem 2 (2009) 719–730.
[19] M. Massa, A. Andersson, E. Finocchio, G. Busca, J. Catal. 307 (2013) 170–184.

[20] A. Witsuthammakul, T. Sooknoi, Appl. Catal. A 413–414 (2012) 109–116.
[21] Y.T. Kim, K.D. Jung, E.D. Park, Appl. Catal. B 107 (2011) 177–187.
[22] P. Laurio-Garbay, J.M.M. Millet, S. Loridant, V. Bellière-Baca, P. Rey, J. Catal. 280 (2011) 68–76.
[23] M. Massa, A. Andersson, E. Finocchio, G. Busca, F. Lenrick, L.R. Wallenberg, J. Catal. 297 (2013) 93–109.
[24] D.H. Olson, G.T. Kokotailo, S.L. Lawton, W.M. Meler, J. Phys. Chem. 85 (1981) 2238–2243.
[25] Y. Choi, Y.S. Yun, H. Park, D.S. Park, D. Yun, J. Yi, Chem. Commun. 50 (2014) 7652–7655.
[26] E. Yoda, A. Ootawa, Appl. Catal. A 360 (2009) 66–70.
[27] S.-H. Chai, H.-P. Wang, Y. Liang, B.-Q. Xu, Green Chem. 9 (2007) 1130–1136.
[28] E. Tsukuda, S. Sato, R. Takahashi, T. Sodesawa, Catal. Commun. 8 (2007) 1349–1353.
[29] A. Corma, G.W. Huber, L. Sauvanaud, P. O'Connor, J. Catal. 257 (2008) 163–171.
[30] L. Qadariyah, Mahfud, Sumarno, S. Machnudah, Wahyudiono, M. Sasaki, M. Goto, Bioresour. Technol. 102 (2011) 9267–9271.
[31] B.O. Dalla Costa, M.A. Peralta, C.A. Querini, Appl. Catal. A 472 (2014) 53–63.
[32] N.M. Ostrovskii, Kinet. Catal. 46 (2005) 737–748.
[33] J. Barrault, Y. Pouilloux, J.M. Clacens, C. Vanhove, S. Bancquart, Catal. Today 75 (2002) 177–181.
[34] C.H. Bartholomew, Appl. Catal. A 212 (2001) 17–60.
[35] M. Guisnet, P. Magnoux, Appl. Catal. A 212 (2001) 83–96.
[36] E. Epelde, M. Ibañez, A.T. Aguayo, A.G. Gayubo, J. Bilbao, P. Castaño, Micropor. Mesopor. Mater. 195 (2014) 284–293.
[37] M. Ibañez, M. Artetxe, G. Lopez, G. Elordi, J. Bilbao, M. Olazar, P. Castaño, Appl. Catal. B 148–149 (2014) 436–445.
[38] D.M. Bibby, R.F. Howe, G.D. McLellan, Appl. Catal. A 93 (1992) 1–34.
[39] J. Kim, M. Choi, R. Ryoo, J. Catal. 269 (2010) 219–228.
[40] C.E. Snape, B.J. McGhee, S.C. Martin, J.M. Andresen, Catal. Today 37 (1997) 285–293.
[41] P. Castaño, G. Elordi, M. Olazar, A.T. Aguayo, B. Pawelec, J. Bilbao, Appl. Catal. B 104 (2011) 91–100.
[42] J.L. Bonardet, M.C. Barrage, J. Fraissard, J. Molec, J. Mol. Catal. A: Chem. 96 (1995) 123–143.
[43] E. Simón, J.M. Rosas, A. Santos, A. Romero, Chem. Eng. J. 214 (2013) 119–128.
[44] M. Rozwadowski, M. Lezanska, J. Wloch, K. Erdmann, R. Golembiewski, J. Kornatowski, Chem. Mater. 13 (2001) 1609–1616.
[45] J. Barrault, J.-M. Clacens, Y. Pouilloux, Top. Catal. 27 (2004) 137–142.